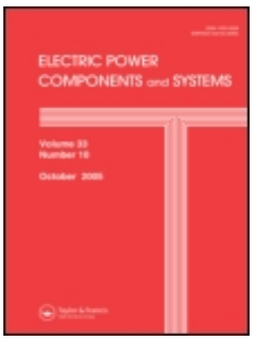

Taylor & Francis
Taylor & Francis Group

Electric Power Components and Systems

ISSN: 1532-5008 (Print) 1532-5016 (Online) Journal homepage: http://www.tandfonline.com/loi/uemp20

Out-of-step Detection Using Energy Equilibrium Criterion in Time Domain

Sumit Paudyal , Ramakrishna Gokaraju , Mohindar S. Sachdev & Shengli Cheng

To cite this article: Sumit Paudyal , Ramakrishna Gokaraju , Mohindar S. Sachdev & Shengli Cheng (2009) Out-of-step Detection Using Energy Equilibrium Criterion in Time Domain, Electric Power Components and Systems, 37:7, 714-739, DOI: 10.1080/15325000902762208

To link to this article: https://doi.org/10.1080/15325000902762208

Electric Power Components and Systems, 37:714–739, 2009

ISSN: 1532-5008 print/1532-5016 online
DOI: 10.1080/15325000902762208

Taylor & Francis
Taylor & Francis Group

Out-of-step Detection Using Energy Equilibrium Criterion in Time Domain

SUMIT PAUDYAL,[1] RAMAKRISHNA GOKARAJU,[1] MOHINDAR S. SACHDEV,[1] and SHENGLI CHENG[1]

[1]Department of Electrical and Computer Engineering, University of Saskatchewan, Saskatoon, Canada

Abstract *This article introduces a new algorithm to detect the out-of-step condition in a power system based on energy equilibrium criterion in the time domain. The proposed energy equilibrium criterion is developed using the concept of equal area criterion in the power-angle domain, and it eliminates the numerical computations required to find the critical clearing time to detect the out-of-step condition. The proposed algorithm detects the out-of-step condition based on the real-time transient energy information available from the local substations. The effectiveness of the proposed algorithm is tested on a single-machine infinite-bus system, a two-machine infinite-bus system, and a three-machine infinite-bus system. The performance of the proposed algorithm is compared with an existing concentric rectangle scheme. The simulation results show that the proposed algorithm can be applied to larger systems and is faster compared to the concentric rectangle scheme.*

Keywords power system relaying, power system stability, equal area criterion

1. Introduction

Power swings are due to perturbations such as changes in load and faults on the system. These perturbations lead to fluctuations of voltages, currents, and power flows [1]. Power swings are of two types: unstable and stable swing. The unstable swing causes excessive power fluctuations and may drive the system to instability. This is commonly known as the out-of-step condition. On the other hand, for a stable swing, the power fluctuation damps out and the system restores to a steady state [1].

Power swing affects the relays in different ways. Distance relays, instantaneous overcurrent relays, time overcurrent relays, and directional instantaneous overcurrent relays may operate during the power swing, but distance relays are the most susceptible [2]. This is because, irrespective of whether it is a stable swing or out-of-step condition, oscillation of voltage and current during the power swing causes the distance relay to

Received 21 March 2008; accepted 9 January 2009.
Address correspondence to Dr. Ramakrishna Gokaraju, Department of Electrical and Computer Engineering, University of Saskatchewan, Engineering Building, 57 Campus Drive, Saskatoon, S7N 5A9, Canada. E-mail: rama.krishna@usask.ca

operate if the measured impedance enters the operating characteristic of the relay. The relays mentioned above should not trip during a stable power swing; they all should allow the power system to return to a stable operating condition. Relays that are likely to operate during the stable power swing should be temporarily blocked to prevent system separations [2]; this is the objective of out-of-step relaying.

Conventional out-of-step relaying practices use impedance measurement units with different shapes of relay characteristics in impedance plane. Depending on the shape in the impedance plane, the scheme may be a blinder scheme, a concentric circle scheme, a concentric polygon scheme, or a lenticular scheme [1, 3]. Selection of a scheme depends on the load pattern, the power system parameters, and the desired performance; however, the main algorithm for their operation is the same. These schemes discriminate fault and power swing based on the apparent impedance seen by the relay. The impedance seen by the relay changes slowly during the swing in comparison to a faulted case [3]. To implement these schemes, extensive system studies were needed, and the schemes ensured proper protection only in the worst case scenarios [4]. Besides this, these schemes were not able to distinguish a swing from a fault when the impedance seen by the relay changed quickly [5].

Another method that overcame the shortcomings of the impedance-based method was the rate of change of apparent resistance augmentation [6]. This method required settings of resistance and time parameters for the relay. The selection of the parameters was not straightforward and depends on the power system parameters. This method worked satisfactorily if the protection equipments were installed close to the oscillation center [4].

Various electrical signals—bus voltage, transmission line current, and active and reactive powers, which were useful for out-of-step detection—were listed in [7]. The electrical signals listed above reflected the power angle indirectly [4]. Protection techniques based on the above signals monitored the oscillations in signals to detect the out-of-step condition, but those techniques could not detect before the power system reached an out-of-step condition.

A swing center voltage (SCV) technique for out-of-step detection was described in [8]. This technique had an advantage—it is independent of system parameters. The estimate of the SCV was from locally available data from the substation; therefore, the estimate was good only when the system impedance angle was close to 90°.

The application of neural networks to predict the out-of-step condition was proposed in [9]. Neural networks have a capability to make a decision quickly for a new case that has close resemblance to a known predefined case for which the neural network is trained. This method needed a large neural network to be trained with different outage cases of the power system; therefore, it made the training process tedious. The neural network suffers from following inherent pitfalls: (i) it makes a quick and correct decision only if it is adequately trained, which is difficult in actual practice; and (ii) it is a black box, and it is difficult to reason out the correct and incorrect decision made. In [10], the application of an artificial intelligence (AI) technique for out-of-step detection was proposed. Similar to the neural network techniques, AI methods also needed a large number of simulations to train the algorithm. The application of fuzzy logic using the adaptive-network-based fuzzy interface (ANFIS) for out-of-step detection is proposed in [11]. This technique used more than one electrical signal—generator output voltages, currents, angular speeds, and powers—so that the decision became more accurate. Unlike the conventional out-of-step relays, such as the concentric rectangular schemes, the methods based on neural network, fuzzy logic, and AI techniques eliminate the need for

adjustments of the relay settings each time the operating condition changes. However, all of them need excessive off-line simulations to train their algorithms.

This article introduces an energy equilibrium criterion in the time domain to detect the out-of-step conditions. The equal area criterion (EAC) concept in the power angle domain is modified to the time domain, and an out-of-step detection algorithm is developed. The proposed algorithm only uses power-flow across transmission line to detect stability and therefore can be implemented using only the local measurements from the substations. The proposed algorithm is independent of the power system parameters and does not need adjustments in the relay settings for any changes in the system parameters. The proposed algorithm is tested on a single-machine infinite-bus (SMIB) system, a two-machine infinite-bus system, and a three-machine infinite-bus system. The performance of the proposed algorithm is compared with a conventional concentric rectangle scheme for out-of-step detection.

2. Proposed Algorithm

Figure 1 shows a SMIB system that will be used to illustrate the traditional EAC and the proposed algorithm. At time t_0 (power angle δ_0), the three-phase fault is applied at the middle of the transmission line TL-II and is cleared at t_c (power angle δ_c) by opening two breakers, A and B, simultaneously.

As already known, the EAC in the power angle domain is useful to analyze system stability without solving the swing equation. The EAC explains the stability of a system based on the area under the power curves in the P-δ plane. However, we still need to solve the swing equation to find the critical clearing time [12]. Solutions of the swing equation using numerical integration techniques, such as the Euler and Runge Kutta methods, give δ as a function of time [13].

2.1. *Energy Equilibrium Criterion in Time Domain*

Instead of analyzing the stability in the power-angle (P-δ) plane, the proposed energy equilibrium criterion describes the stability of a system in a power-time (P-t) plane. This method gathers P-t information from the local substations and calculates the area during the transient to detect the out-of-step condition. The area under a P-t curve gives the information of energy; thus, the proposed method can be viewed as an energy equilibrium criterion. This section briefly describes the steps to get the mathematical expressions for the energy equilibrium criterion in the time domain starting from the

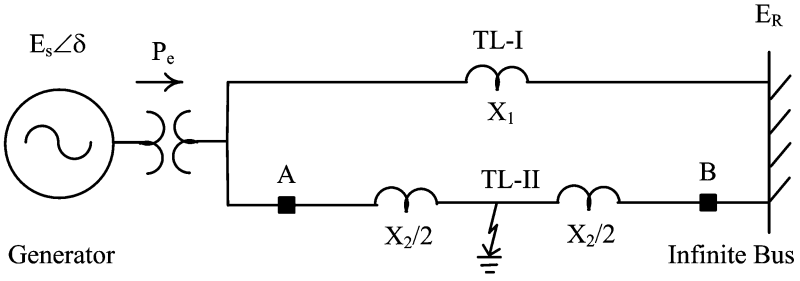

Figure 1. A SMIB system.

swing equation (Eq. (1)) [14]:

$$\frac{M}{\omega_s}\frac{d^2\delta}{dt^2} = P_m - P_e = \Delta P, \tag{1}$$

where M is the generator inertia constant, P_m is the input mechanical power, P_e is the output electrical power, and ω_s is the system frequency [13]. Speed deviation ω_r is given by

$$\omega_r = \omega(t) - \omega_s = \frac{d\delta}{dt}. \tag{2}$$

Using Eqs. (1) and (2), we get

$$\frac{M}{\omega_s} d\omega_r = (P_m - P_e)dt. \tag{3}$$

By integrating Eq. (3),

$$\frac{M}{\omega_S}\int d\omega_r = \int (P_m - P_e)dt. \tag{4}$$

Acceleration area A_1 is obtained from Eq. (4) by setting the limit of integration from t_0 to t_c (see Eq. (5)). As stated before, t_0 is the time of inception of the fault, and t_c is the fault clearing time. Note that at t_0, the speed deviation is zero because the speed of the rotor is the synchronous speed;

$$A_1 = \int_{t_0}^{t_c} (P_m - P_e)dt = \frac{M}{\omega_s}(\omega_r|_{t_c} - \omega_r|_0). \tag{5}$$

Similarly, deceleration area A_2 is obtained from Eq. (4) by setting the limit of integration from t_c to $t_{\max}$ (see Eq. (6)). Time $t_{\max}$ for a stable case represents the time corresponding to the maximum swing of power angle ($\delta = \delta_{\max}$), and for an unstable case, it is the time when the power angle swings beyond the deceleration region ($\delta = \pi - \delta_0$):

$$A_2 = \int_{t_c}^{t_{\max}} (P_m - P_e)dt = \frac{M}{\omega_s}(\omega_r|_{t_{\max}} - \omega_r|_{t_c}). \tag{6}$$

For a stable system at $t_{\max}$, the speed of the rotor is synchronous speed, so the speed deviation is zero, but for the out-of-step condition, the speed of the rotor at $t_{\max}$ is not synchronous speed. So the total area for stable and out-of-step conditions is given as follows:

For the stable condition:

$$A = A_1 + A_2 = \int_{t_0}^{t_{\max}} (P_m - P_e)dt = 0. \tag{7}$$

For the out-of-step condition:

$$A = A_1 + A_2 = \int_{t_0}^{t_{\max}} (P_m - P_e)dt > 0. \tag{8}$$

If we approximate the integration by summation and assume input mechanical power is equal to pre-fault electric power, the above equations can be rewritten as follows:

For the stable condition:

$$\sum_{t_0}^{t_1}(P_e|_{t_0-\Delta t} - P_e)\Delta t = 0. \tag{9}$$

For the out-of-step condition:

$$\sum_{t_0}^{t_{\max}}(P_e|_{t_0-\Delta t} - P_e)\Delta t > 0. \tag{10}$$

Equations (9) and (10) represent the energy that is the area under the *P-t* curve and the basis of the proposed algorithm. If there is a balance of accelerating and decelerating energy in the system during the transient, the system becomes stable. An unbalance of transient energy leads the system to the out-of-step condition. The flowchart of the proposed algorithm based on Eqs. (9) and (10) is shown in Figure 2.

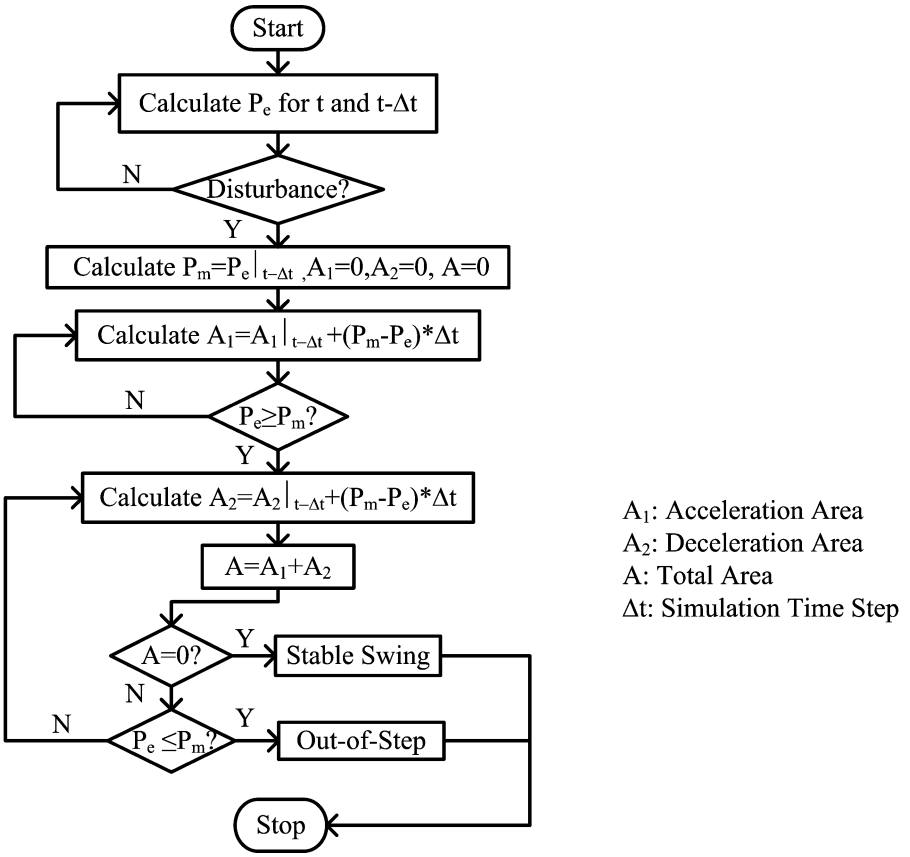

Figure 2. Flowchart of the proposed algorithm.

2.2. Nature of P-t Curves

The energy equilibrium criterion describes the stability based on the *P-t* curves. The nature of the *P-t* curve depends on the swing of δ after disturbance. For a stable system, δ can swing less than 90°, equal to 90°, or more than 90°. For an unstable system, δ always swings beyond 90°. Therefore, in general, three types of *P-t* curves are possible:

- a *P-t* curve for a stable system with a swing of $\delta \leq 90°$,
- a *P-t* curve for a stable system with a swing of $\delta > 90°$, and
- a *P-t* curve for an unstable system.

The possible nature of *P-t* curves are presented in the following section. Actual *P-t* curves obtained from simulations will be explained later in Section 3.

2.2.1. P-t Curve for a Stable System with Swing $\delta \leq 90°$. A P-δ curve for a stable system with swing of $\delta < 90°$ is shown in Figure 3. In the acceleration region of the P-δ curve, $P_m > P_e$, where P_m is input mechanical power and P_e is output electrical power in the deceleration region $P_e > P_m$. During the transient, the locus in the P-δ plane follows the path a to b to c to d to e to d. Note that the swing is from d to e and back to d in the deceleration region. The maximum power during the transient condition corresponds to point e, *i.e.*, the power at maximum swing of $\delta = \delta_{\max}$. If the acceleration area A_1 is less than the deceleration area available up to $\pi - \delta_0$, then the system is said to be stable. For this condition, δ swings up to $\delta_{\max}$ such that area A_1 equals the deceleration area up to $\delta_{\max}$ (area A_2) [12].

The corresponding *P-t* curve for Figure 3 is shown in Figure 4. The analysis of the curve in the deceleration region reveals that the *P-t* curve is one-peaked (see point e) with the maximum value of power corresponding to the maximum swing of $\delta = \delta_{\max}$. As stated before, swing in deceleration region is from d to e and back to d, and therefore, the *P-t* curve in the deceleration region is symmetrical about point e. The nature of

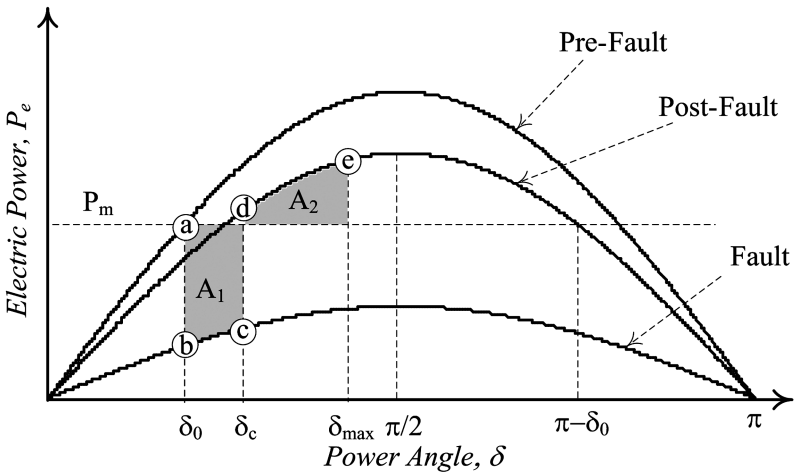

Figure 3. P-δ curve for a stable system with swing of $\delta < 90°$.

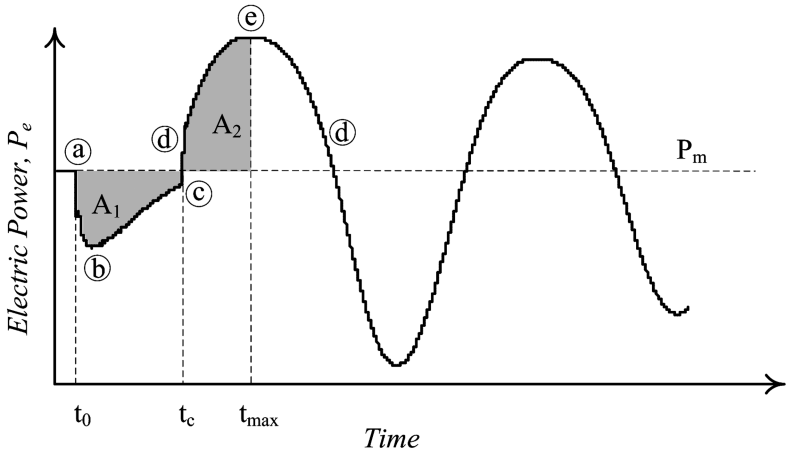

Figure 4. *P-t* curve for a stable system with swing of $\delta < 90°$.

the *P-t* curve for a system with the maximum swing of $\delta = 90°$ will be similar to Figure 4, except that the maximum power at point *e* corresponds to the power at $\delta = 90°$.

2.2.2. P-t Curve for a Stable System with Swing of $\delta > 90°$. A P-δ curve for a stable system with swing of $\delta > 90°$ is shown in Figure 5. After disturbance, the locus in the P-δ plane follows the path *a* to *b* to *c* to *d* to *e* to *f* to *e* to *d*. Note that the locus crosses $\delta = 90°$ at *e*, reaches up to *f*, and then swings backs to *e*.

The corresponding *P-t* curve for Figure 5 is shown in Figure 6. The *P-t* curve has two peaks in the decelerating region corresponding to the power at $\delta = 90°$. The minimum power between the two peaks corresponds to the power at $\delta = \delta_{max}$. The curve in the deceleration region is symmetrical about point *f*.

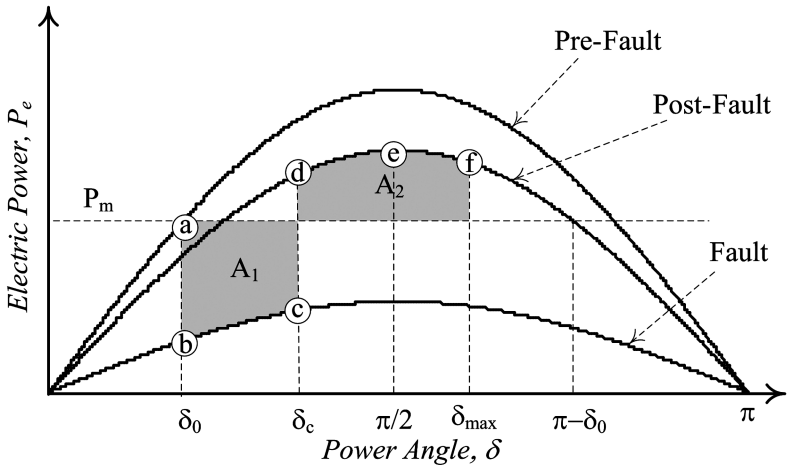

Figure 5. P-δ curve for a stable system with swing of $\delta > 90°$.

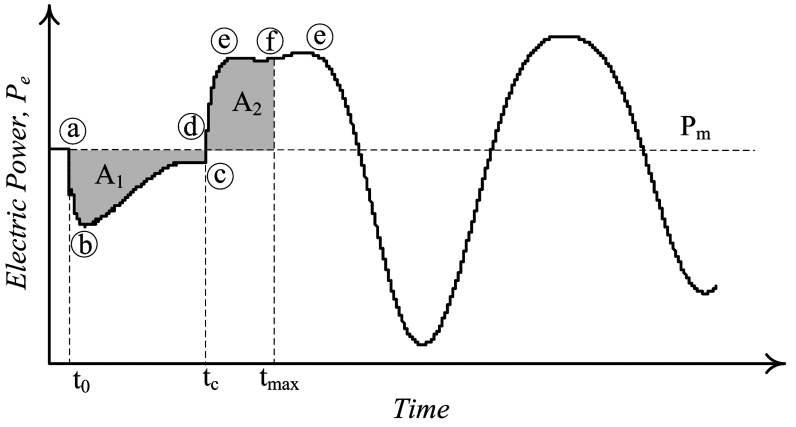

Figure 6. *P-t* curve for a stable system with swing of $\delta > 90°$.

2.2.3. P-t Curve for an Unstable System. A P-δ curve for an unstable system is shown in Figure 7. After disturbance, the locus in the P-δ plane follows the path a to b to c to d to e to f to g. Note that the locus crosses $\delta = 90°$ at e and never swings back. For an unstable system, the maximum deceleration area A_2 is always less than the acceleration area A_1 [12].

The corresponding *P-t* curve for the unstable system is shown in Figure 8. The maximum power corresponds to the power at $\delta = 90°$. As mention earlier, δ never swings back after it crosses $\delta = 90°$, and therefore, the curve is not symmetrical in the declaration region.

In summary, a stable system can have one- or two-peaked power curves in the deceleration region, and the curves are symmetrical about the peak power. An unstable system always has a one-peaked *P-t* curve in the deceleration region and is not symmetric.

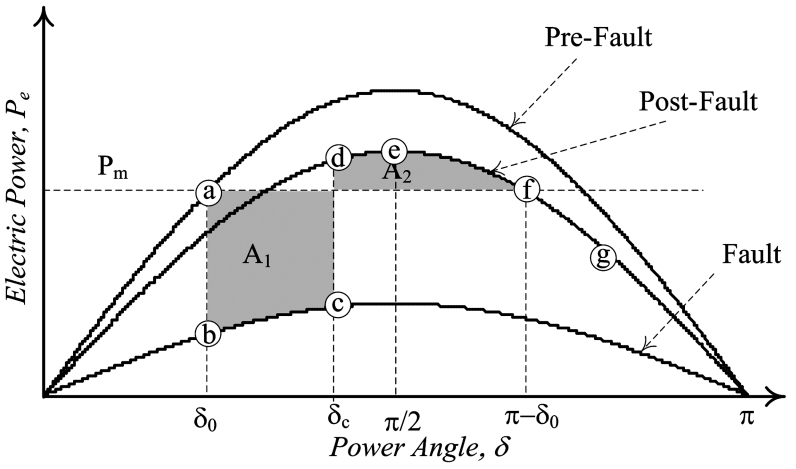

Figure 7. P-δ curve for an unstable system.

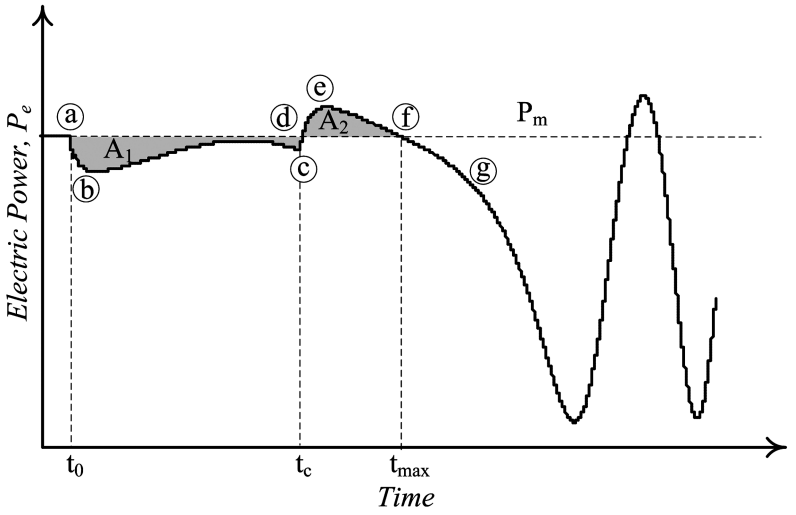

Figure 8. *P-t* curve for an unstable system.

3. Simulation

3.1. SMIB Simulation

A power system as shown in Figure 1 is used first to test the proposed algorithm for a SMIB system [15]. The system parameters are given in Appendix A. Different power swings are obtained by applying a three-phase fault at the middle of a transmission line (TL-II) and clearing the fault by opening breakers A and B simultaneously at two ends of the transmission line. Stable and out-of-step swings are obtained by operating the power system at different pre-fault conditions and varying the fault duration time. The power system transient simulation tool PSCAD^{TM} (Manitoba HVDC Research Centre, Winnipeg, Canada) is chosen for the simulation.

3.1.1. Stable Cases. Five different scenarios were used for the stable case studies. In the first case, small pre-fault load and small fault clearing time was used. In the successive cases, pre-fault load and fault clearing time were increased to obtain various stable swing scenarios. Figure 9 shows a case with the pre-fault $\delta = 25°$ and the fault cleared after 10 cycles (0.167 sec). The total accelerating area A_1 is 0.035 p.u. After 0.5 sec, the total area A becomes zero in the decelerating region. Thus, this case is concluded as a stable swing. Also note that the maximum deceleration area available is 0.070 p.u., which is more than area A_1.

Figure 10 shows another simulation case in which the pre-fault δ is kept constant and the fault clearing time is increased to 12 cycles (0.2 sec). As fault clearing time is more compared to the previous case, acceleration area A_1 (0.040 p.u.) is also more; it takes 0.51 sec to decide that it is a stable swing.

Next, the pre-fault δ is increased to 30° and the fault is cleared after 8 cycles (0.133 sec). The *P-t* curve is shown in Figure 11. Decision is made at 0.59 sec that it is a stable swing.

Keeping the pre-fault δ the same, the next fault clearing time is increased to 10 cycles (0.167 sec). The acceleration area is greater compared to the previous case, so it takes

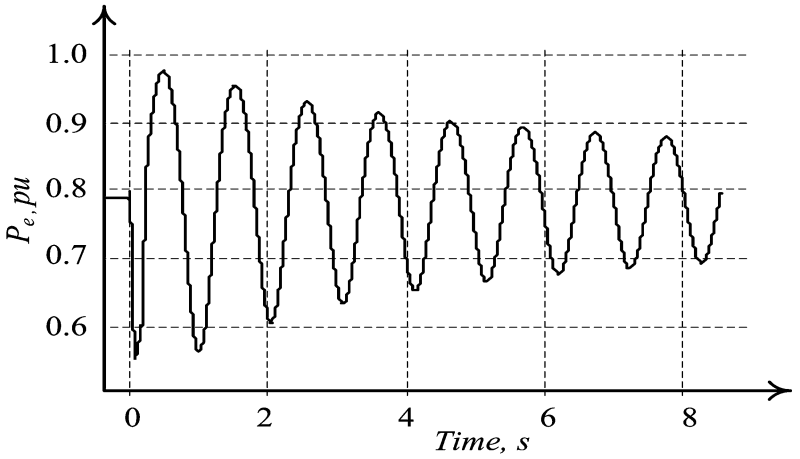

Figure 9. *P-t* curve for pre-fault $\delta = 25°$ and cleared after 10 cycles.

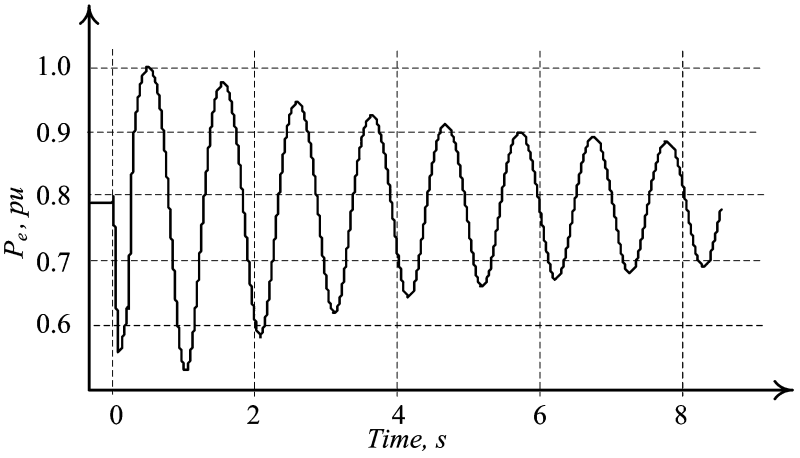

Figure 10. *P-t* curve for pre-fault $\delta = 25°$ and cleared after 12 cycles.

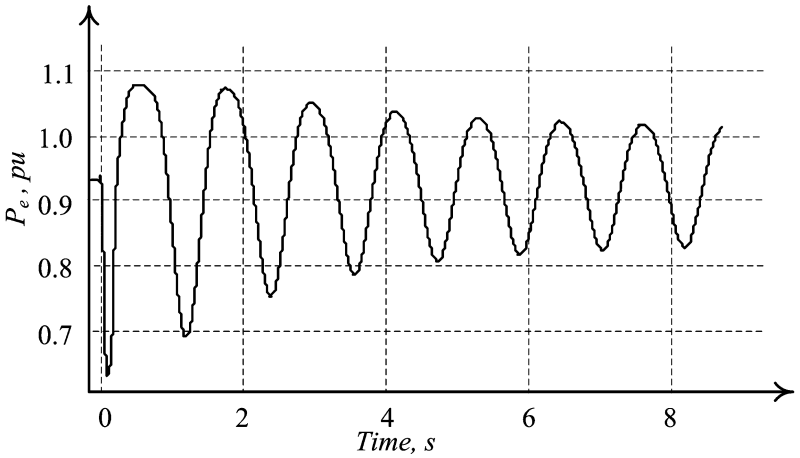

Figure 11. *P-t* curve for pre-fault $\delta = 30°$ and cleared after 8 cycles.

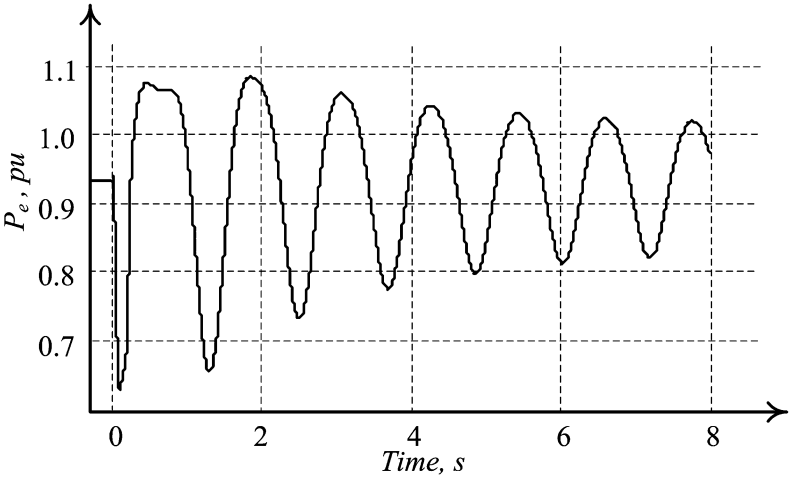

Figure 12. *P-t* curve for pre-fault $\delta = 30^\circ$ and cleared after 10 cycles.

more time to make the decision. Figure 12 shows the *P-t* curve for this case. The decision is made that it is stable swing at 0.64 sec.

By further increasing the fault clearing time to 12 cycles (0.2 sec), large oscillations in swing are observed, as shown in Figure 13. It takes 0.85 sec to decide the swing is a stable swing. The time taken is larger than the previous case because the acceleration area is increased. The results of above five simulation cases are summarized in Table 1.

Among the five stable cases, the *P-t* curves of the first three cases are one-peaked and symmetric about the peak in the deceleration region. The *P-t* curves for the rest of the three cases are two-peaked in the deceleration region. A *P-t* curve having two peaks in deceleration region is always stable. The frequencies of the swings encountered during the simulation are in the range of 0.8 to 1 Hz.

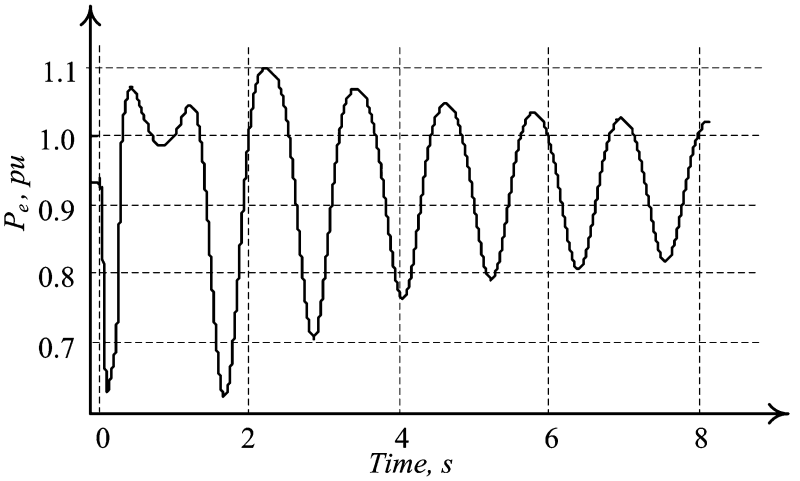

Figure 13. *P-t* curve for pre-fault $\delta = 30^\circ$ and cleared after 12 cycles.

Table 1
Summary of simulation results for stable power swing

	Case				
	1	2	3	4	5
Power angle δ (°)	25	25	30	30	30
Fault duration cycles	10	12	8	10	12
Fault duration time (sec)	0.167	0.20	0.133	0.167	0.20
Acceleration area A_1 (p.u.)	0.035	0.040	0.041	0.048	0.054
Deceleration area A_2 (p.u.)	−0.035	−0.040	−0.041	−0.048	−0.054
Maximum deceleration area (p.u.)	−0.070	−0.080	−0.081	−0.092	−0.099
$A = A_1 + A_2$	0	0	0	0	0
Decision time (sec)	0.5	0.51	0.59	0.64	0.85
Swing frequency (Hz)	0.8–1.0				

3.1.2. Out-of-step Cases. Five different simulations are reported here to demonstrate the out-of-step detection using the proposed algorithm. Starting with the stable simulation cases, fault clearing time is increased to obtain out-of-step conditions. Figure 14 shows a *P-t* curve with a pre-fault $\delta = 30°$, and the fault is cleared after 14 cycles (0.233 sec). The acceleration area is 0.061 p.u., and the maximum available deceleration area is 0.027 p.u. In the first swing, the total area calculated is not zero, so this is an out-of-step condition that is decided at 0.598 sec.

Figure 15 shows the *P-t* curve for a fault clearing time of 16 cycles (0.267 sec). The acceleration area increases to 0.067 p.u., and the out-of-step condition is detected at 0.504 sec. Note that the decision made is faster compared to the previous case because the maximum deceleration area has reduced to 0.016 p.u.

Figure 16 shows the *P-t* curve for another case with fault duration time of 18 cycles (0.3 sec). The acceleration area increases to 0.073 p.u., and the deceleration area drops to 0.008 p.u. The out-of-step decision is made at 0.466 sec.

In another study, the pre-fault δ is increased to 35°, and the two simulations are carried out with fault duration times of 8 and 10 cycles. The *P-t* curves are shown in Figures 17 and 18, respectively. When the fault duration time is 8 cycles (0.133 sec), the acceleration area is 0.050 p.u., and the deceleration area is 0.031 p.u. The out-of-step condition is detected at 0.76 sec, and the total area is 0.0194 p.u. In the second case, the fault duration time is 10 cycles (0.167 sec), which results in a larger acceleration area of 0.057 p.u. The deceleration area is 0.019 p.u. Compared to the previous study, the deceleration area is smaller, so the decision is made faster. It takes 0.554 sec to make the decision that it is out-of-step. The simulation results are summarized in Table 2.

Overall, the analysis of the *P-t* curves shows that the out-of-step curves are one-peaked curves in the deceleration region and the curves are not symmetric about the peak power. The frequency of swing measured in these simulations is in the range of 4–6 Hz. For the kind of synchronous machine that is used in the simulation, it is not possible to get swing frequencies larger than 6 Hz. However, as the proposed algorithm is based only on the areas, the swing frequency should not affect the accuracy of the algorithm. Therefore, this algorithm would work for a larger frequency of swings as well.

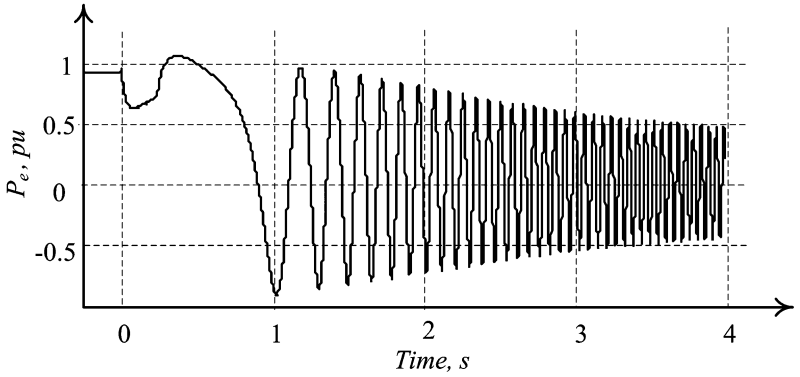

Figure 14. *P-t* curve for pre-fault at $\delta = 30°$ and cleared after 14 cycles.

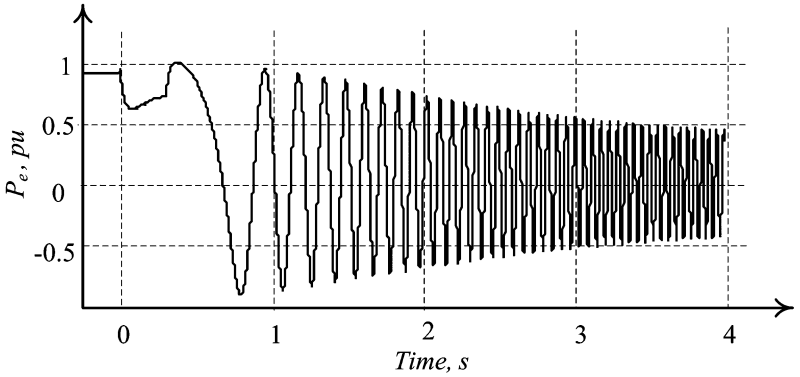

Figure 15. *P-t* curve for pre-fault $\delta = 30°$ and cleared after 16 cycles.

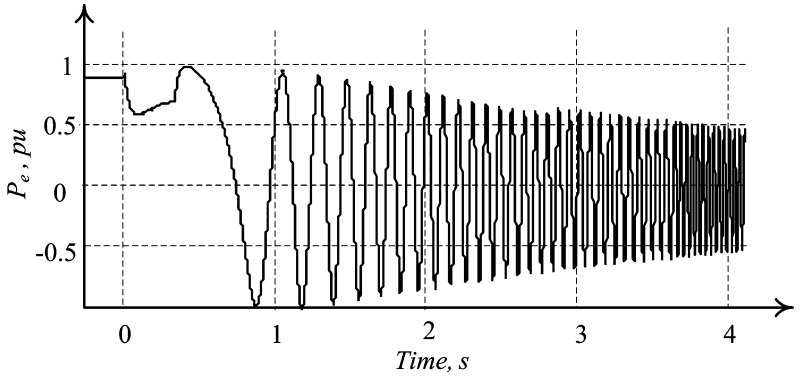

Figure 16. *P-t* curve for pre-fault $\delta = 30°$ and cleared after 18 cycles.

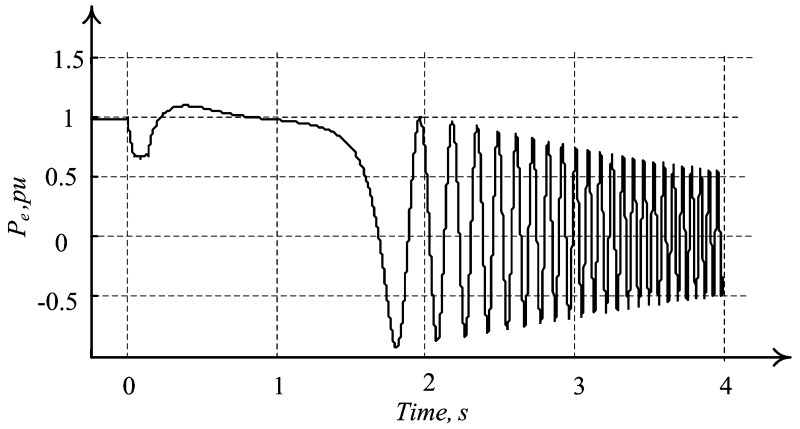

Figure 17. *P-t* curve for pre-fault $\delta = 35°$ and cleared after 8 cycles.

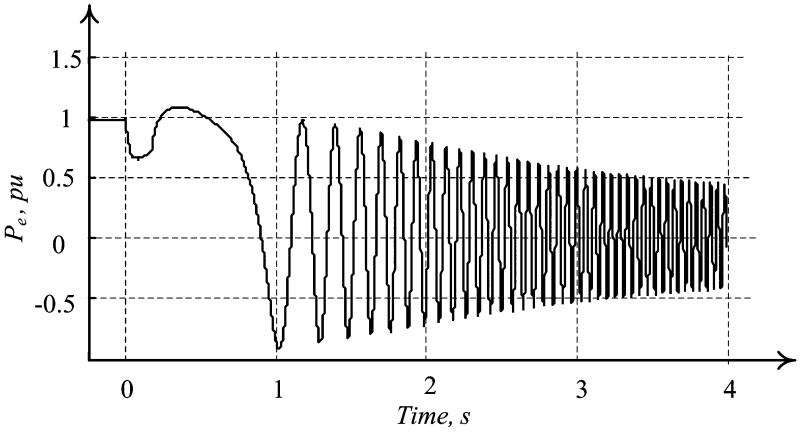

Figure 18. *P-t* curve for pre-fault $\delta = 35°$ and cleared after 10 cycles.

Table 2
Summary of simulation results for out-of-step cases

	Case				
	1	2	3	4	5
Power angle δ (°)	30	30	30	35	35
Fault duration cycles	14	16	18	8	10
Fault duration time (sec)	0.233	0.267	0.30	0.133	0.167
Acceleration area A_1 (p.u.)	0.061	0.067	0.073	0.050	0.057
Deceleration area A_2 (p.u.)	−0.027	−0.016	−0.008	−0.031	−0.019
Maximum deceleration area (p.u.)	−0.027	−0.016	−0.008	−0.031	−0.019
$A = A_1 + A_2$	0.033	0.051	0.065	0.019	0.038
Decision time (sec)	0.598	0.504	0.466	0.760	0.554
Swing frequency (Hz)	4–6				

Table 3
Summary of simulation for the comparison of decision time

	Case					
	1	2	3	4	5	6
Power angle δ (°)	30	30	30	30	30	30
Fault duration cycles	8	10	12	14	16	18
Fault duration time (sec)	0.133	0.167	0.20	0.23	0.26	0.30
Acceleration area A_1 (p.u.)	0.041	0.048	0.054	0.061	0.067	0.073
Deceleration area A_2 (p.u.)	−0.041	−0.048	−0.054	−0.027	−0.016	−0.008
Decision time (sec)	0.59	0.64	0.85	0.598	0.504	0.466
Decision	Stable	Stable	Stable	Out-of-step	Out-of-step	Out-of-step

3.1.3. Comment on the Decision Time. This section explains the effect of disturbance on the acceleration and deceleration areas of the *P-t* curve and in decision-making. A comparison is done based on the simulations carried out in the previous sections for pre-fault $\delta = 30°$. Decision times for various fault clearing cycles are listed in Table 3.

In Table 3, cases 1 through 3 are for the stable swing and cases 4 through 6 are for the out-of-step condition. For stable cases, when the fault duration time is increased from 8 to 12 cycles, the acceleration area increases from 0.041 to 0.054 p.u. The larger the acceleration area, the larger the deceleration area to make the total area zero. The time taken to make a decision increases from 0.59 to 0.85 sec. For the out-of-step condition, the acceleration area increases from 0.061 to 0.0734 p.u, but the deceleration area decreases from 0.027 to 0.008 p.u. Therefore, it requires less time to calculate the deceleration area. This reduces the decision time from 0.598 to 0.466 sec.

Stable swings with smaller oscillations are obtained when pre-fault δ is small and the fault is cleared as quickly as possible. The acceleration area for such stable swings becomes less (see Figure 7). It is not necessary to wait longer in the deceleration region to obtain the total area equal to zero. Thus, the algorithm is able to make the decisions quickly. For the out-of-step condition with a larger pre-fault load and larger fault duration, the acceleration region becomes large, but the deceleration region becomes very small. So the decision can still be made quickly. But when the swing is marginally stable or marginally unstable, the acceleration, as well as deceleration, areas become comparable, so it takes more time to make the decision.

3.1.4. Comparison of the Proposed Algorithm with the Concentric Rectangle Scheme. When proposing a new relaying algorithm for protection, it is useful to compare it with an available standard practice in literature for relaying. In this article, the performance of the proposed out-of-step detection algorithm is compared with the concentric rectangle scheme [7]. Figure 19 shows a concentric rectangle scheme in which the time taken by impedance seen by the relay to traverse inner and outer rectangles is compared with the pre-set time to discriminate between the fault and swing. If the swing locus traverses inner and outer rectangles in less than the pre-set time, the disturbance is a fault. If the locus enters the outer rectangle and takes more than the pre-set time to cross the inner rectangle, then it is an out-of-step condition. If the swing locus crosses the outer rectangle but does not cross the inner rectangle, the swing is a stable swing [7].

For performance comparison, an impendence relay with concentric rectangle schemes is located at one end of TL-I (Figure 1), which protects 80% of the line. The power swing

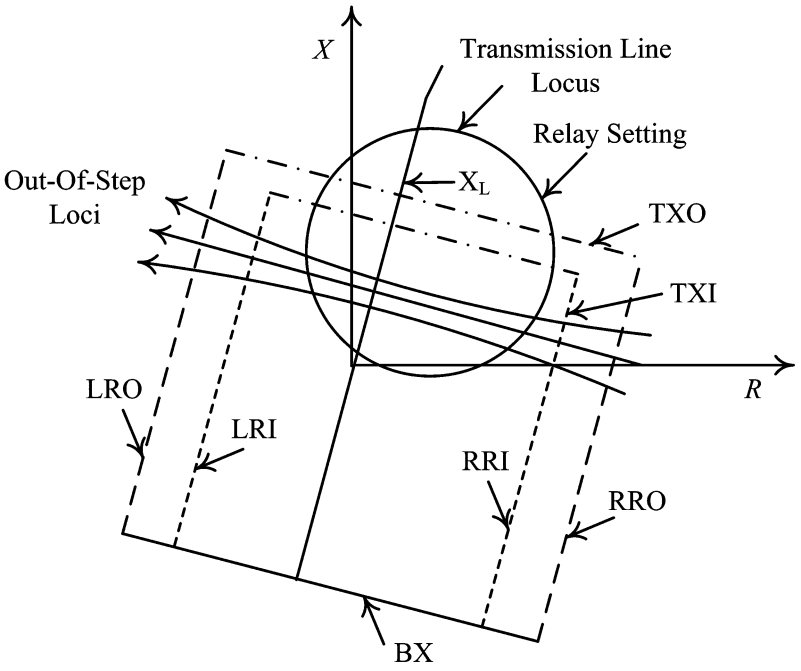

Figure 19. Impedance loci for out-of-step condition and blinder settings.

in TL-I is achieved by applying a fault at the middle of TL-II and simultaneously opening breakers A and B with a different time delay. Detailed guidelines used for relay settings are described in [7]. A brief explanation of the procedure is provided in Appendix B.

In Figure 19,

right resistance—inner (RRI) = 0.3 p.u.
right resistance—outer (RRO) = 0.4 p.u.
left resistance—outer (LRI) = −0.3 p.u.
left resistance—inner (LRO) = −0.4 p.u.
top reactance—inner (TXI) = 0.2 p.u.
top reactance—outer (TXO) = 0.3 p.u.
Bottom rectangles (BX) = −1.94 p.u.

Using the above settings, different simulations are carried out for comparing the proposed algorithm with the concentric rectangle scheme just described.

In the first simulation, the pre-fault power angle is set $\delta = 30^\circ$ and the fault clearing time is set to 14 cycles (0.233 sec). To detect that the system is out-of-step, the concentric rectangular scheme takes 4.93 sec. The locus of the swing is shown in Figure 20. The swing alone takes 27.5 cycles (0.458 sec) to traverse the two concentric rectangles. For this case, the proposed algorithm takes just 0.6 sec to detect that it is out-of-step.

In the next case, the fault clearing time is increased to 16 cycles (0.26 sec). The swing locus takes 20.98 cycles (0.349 sec) to completely traverse the two concentric rectangles, and the decision that it is out-of-step is obtained at 4.70 sec, whereas the proposed algorithm only takes 0.5 sec to make the decision. Increasing the fault clearing time makes the swing more severe; thus, the swing locus traverses the two rectangles in 17.37 cycles (0.289 sec). The concentric rectangle scheme takes 4.58 sec, whereas the

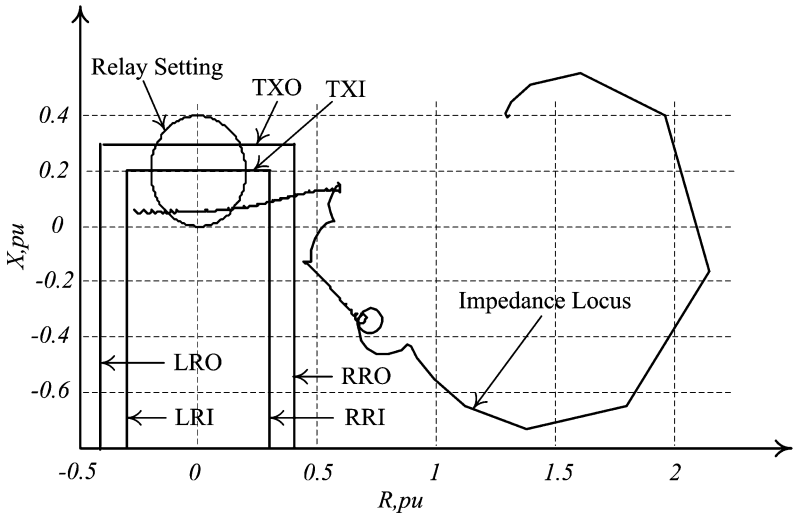

Figure 20. Out-of-step locus for fault duration of 12 cycles and $\delta = 30°$.

Table 4
Comparison of EAC algorithm and concentric rectangle schemes

	Case		
	1	2	3
Pre-fault power angle δ (°)	30	30	30
Fault duration cycles	14	16	18
Fault duration time (sec)	0.23	0.26	0.30
Decision time, rectangle scheme (sec)	4.93	4.70	4.58
Decision time, proposed algorithm (sec)	0.60	0.50	0.47

proposed algorithm takes 0.47 sec to make the decision. The results are summarized in Table 4.

The simulation results show that the proposed algorithm is accurate and much faster compared to the conventional concentric rectangular scheme. Note that the decision time for a concentric rectangular scheme depends on the guidelines used for the relay settings. Besides, finding the required settings for concentric rectangular method is not straightforward. It depends on the system parameters, whereas the proposed algorithm is independent of the system parameters, which is quite an useful advantage.

3.2. Two-machine Infinite-bus Simulation

The effectiveness of the proposed algorithm is also tested on a two-machine infinite-bus system. Figure 21 shows the network configuration of the system, and its parameters are listed in Appendix C. The *P-t* curves of both the generators are monitored, and the

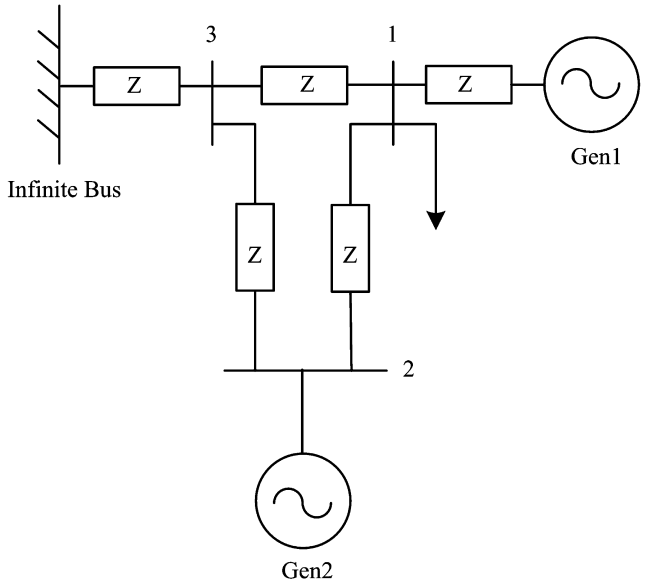

Figure 21. A two-machine infinite-bus system.

proposed algorithm is applied separately to both *P-t* curves. In the simulation studies, it was found that Gen1 did not lead to an out-of-step condition, so the results using Gen1 are not discussed.

3.2.1. Stable Cases. Two simulation cases are reported here for the stable case studies. In the first case, the total load in the system is 0.892 p.u. A three-phase fault is applied at Bus 1 and cleared after 0.1 sec. The *P-t* curves of both the generators are shown in Figure 22. From the *P-t* curve of Gen2, the acceleration area A_1 is 0.0601 p.u. After 0.281 sec, the total area A becomes zero in the decelerating region; thus, this case is

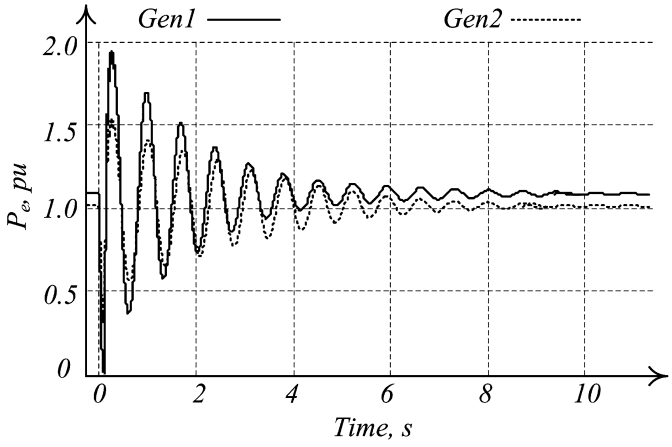

Figure 22. *P-t* curves for pre-fault load of 0.892 p.u. and fault cleared after 0.1 sec.

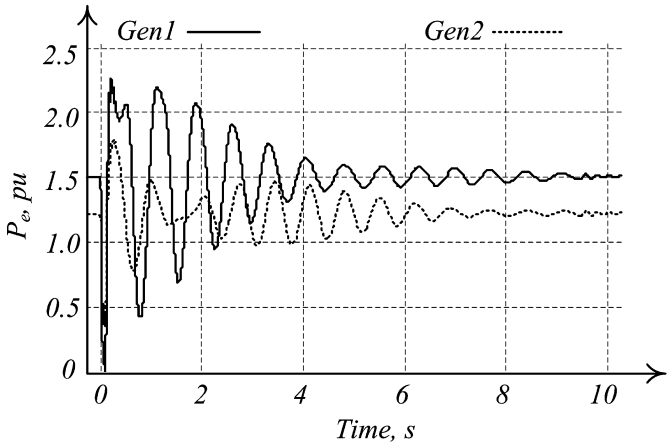

Figure 23. *P-t* curves for pre-fault load of 1.761 p.u. and fault cleared after 0.1 sec.

concluded as a stable swing. Also note that the maximum deceleration area available is 0.1104 p.u. which is more than area A_1.

In the next simulation, the total load in the system is set at 1.761 p.u., and the fault is cleared after 0.1 sec. The *P-t* curves for both generators are shown in Figure 23. From the Gen2's *P-t* curve, the acceleration area A_1 is found to be 0.0778 p.u. The case is decided as a stable case at 0.303 sec when the total area becomes zero.

3.2.2. Out-of-step Cases. Two simulations are carried out to detect the out-of-step condition. In the first simulation case, the total load in the system is set to 0.892 p.u. A three-phase fault is applied at Bus 1 and cleared after 0.25 sec. The *P-t* curves for this simulation case are shown in Figure 24. In Gen2's *P-t* curve, the acceleration area is 0.1511 p.u., and the maximum available deceleration area is 0.0231 p.u. In the first swing, the total area calculated is 0.1280 p.u. This is, therefore, an out-of-step condition, and the decision is made at 0.368 sec.

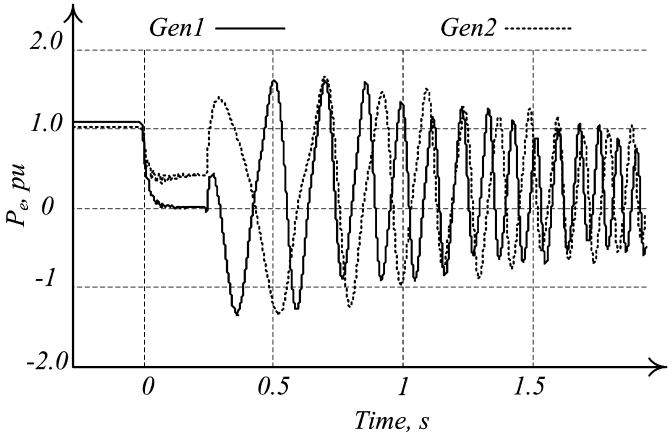

Figure 24. *P-t* curves for pre-fault load of 0.892 p.u. and fault cleared after 0.25 sec.

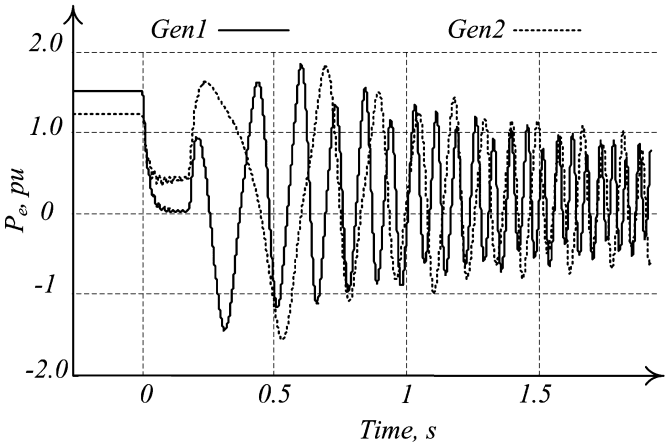

Figure 25. *P-t* curves for pre-fault load of 1.761 p.u. and fault cleared after 0.25 sec.

Table 5
Summary of two-machine infinite-bus simulation results

	Case			
	1	2	3	4
Pre-fault load (p.u.)	0.892	1.761	0.892	1.761
Fault duration time (sec)	0.1	0.1	0.25	0.25
Generator responsible	Gen2	Gen2	Gen2	Gen2
Acceleration area A_1 (p.u.)	0.0601	0.0778	0.1511	0.1404
Deceleration area A_2 (p.u.)	−0.0601	−0.0778	−0.0231	−0.0338
Maximum deceleration area (p.u.)	−0.1104	−0.1333	−0.0231	−0.0338
$A = A_1 + A_2$	0	0	0.1280	0.1066
Decision time (sec)	0.281	0.303	0.368	0.339
Decision	Stable	Stable	Out-of-step	Out-of-step

Figure 25 shows the *P-t* curve for another out-of-step simulation case. The total load is 1.761 p.u., and the fault is cleared after 0.25 sec. In the Gen2's *P-t* curve, the acceleration area A_1 is 0.1404 p.u., and out-of-step condition is detected at 0.339 sec when the maximum deceleration area A_2 is 0.0338 p.u. The summary of stable and out-of-step condition simulation results for the two-machine infinite-bus system are listed in Table 5.

3.3. Three-machine Infinite-bus Simulation

A three-machine infinite-bus system as shown in Figure 26 is considered to illustrate the effectiveness of the algorithm in a more complex power system. The parameters of the system are given in Appendix D. The *P-t* curves of all three generators are monitored, and the proposed algorithm is applied to all of them separately. In the simulation studies,

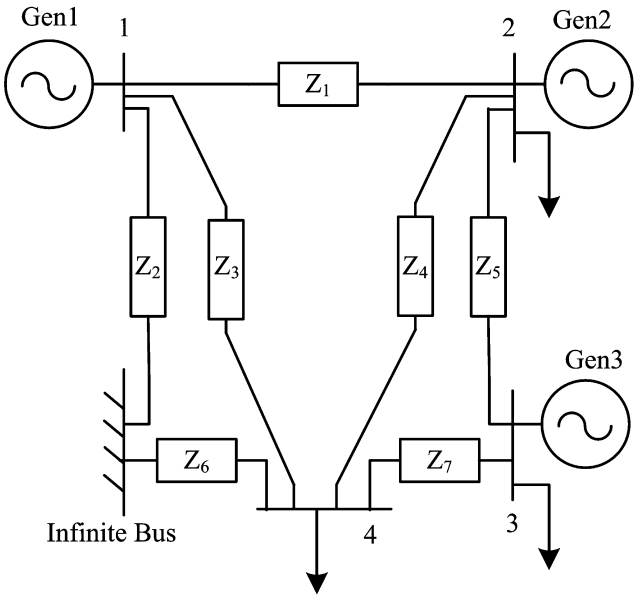

Figure 26. A three-machine infinite-bus system.

it was found that Gen2 led to an out-of-step condition, so the only results using Gen2 are discussed.

3.3.1. Stable Cases. For the first simulation, a three-phase fault is applied at Bus 1. The pre-fault load is 1.569 p.u., and the fault duration is 0.1 sec. The *P-t* curves for the three generators are shown in Figure 27. From the *P-t* curve of Gen2, the acceleration area A_1 is found to be 0.0895 p.u. At 0.346 sec, the total area becomes zero, and a stable swing is decided. The maximum available deceleration area is 0.1427 p.u.

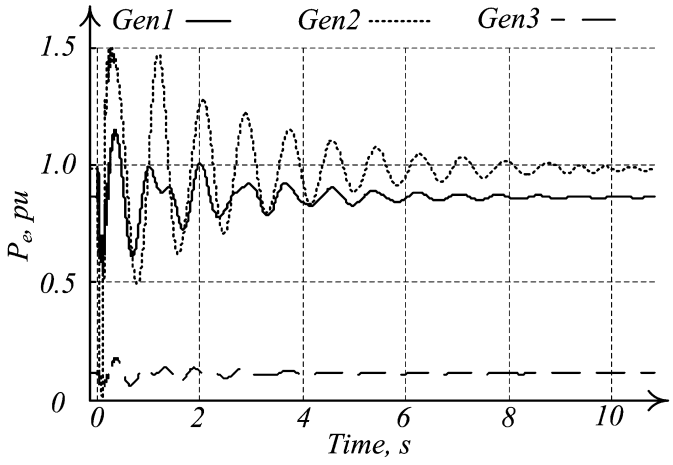

Figure 27. *P-t* curves for pre-fault load of 1.596 p.u. and fault cleared after 0.1 sec.

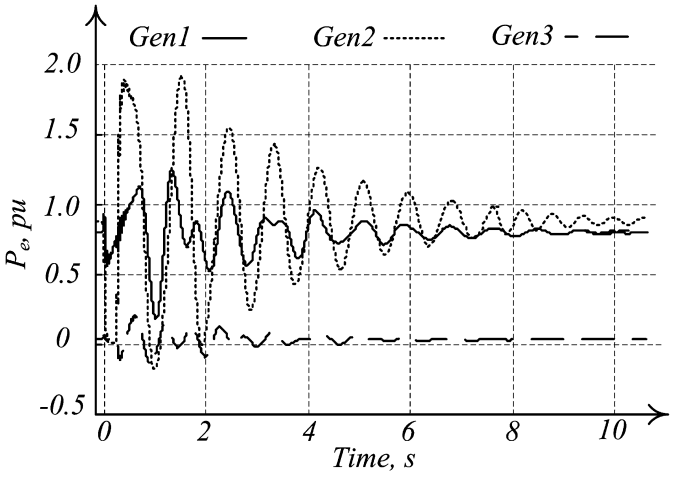

Figure 28. *P-t* curves for pre-fault load of 1.2189 p.u. and fault cleared after 0.25 sec.

The pre-fault load in the system is set at 1.2189 p.u. A three-phase fault is applied at Bus 1, and the fault is cleared after 0.25 sec. The *P-t* curves for this case are shown in Figure 28. From the *P-t* curve of Gen2, the acceleration area A_1 is found to be 0.2127 p.u., and the total area is zero at 0.519 sec. This case is decided as a stable swing, and the maximum available deceleration area is 0.3759 p.u.

3.3.2. Out-of-step Cases. Two simulations are reported here to detect the out-of-step condition using the proposed technique. In the first simulation, the pre-fault load in the system is set at 1.569 p.u., and a three-phase fault is applied at Bus 1 and cleared after 0.25 sec. The *P-t* curves for this simulation are shown in Figure 29. From the *P-t* curve of Gen2, the acceleration area A_1 is 0.2391 p.u., and the maximum available deceleration area is 0.1204 p.u. This case is decided to be an out-of-step condition at 0.536 sec when the total area is 0.1187 p.u.

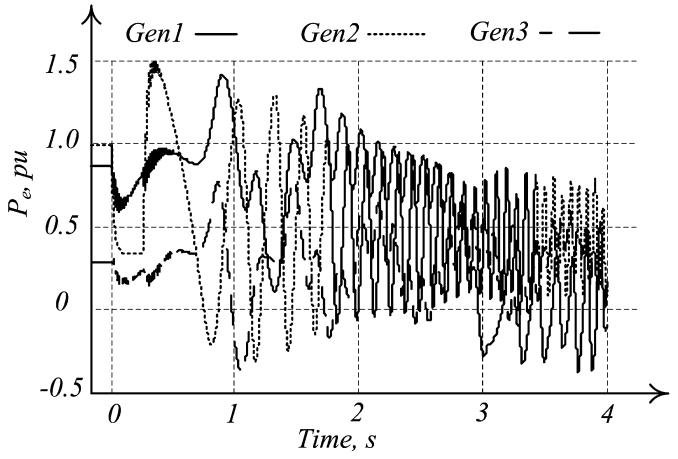

Figure 29. *P-t* curves for pre-fault load of 1.596 p.u. and fault cleared after 0.25 sec.

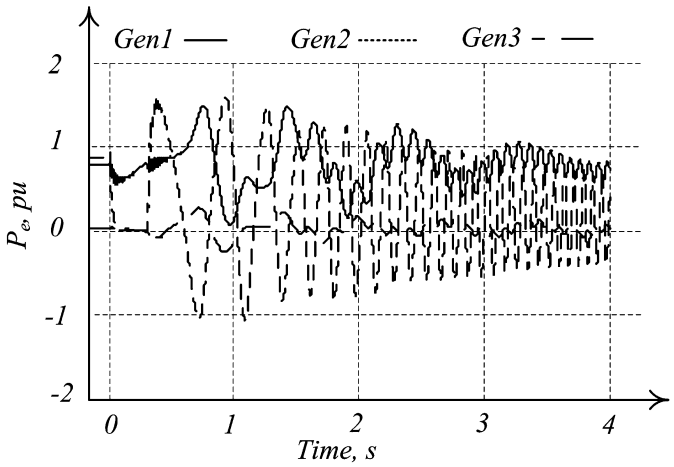

Figure 30. *P-t* curves for pre-fault load of 1.2189 p.u. and fault cleared after 0.30 sec.

In the next simulation, the pre-fault total load is set at 1.2189 p.u. A three-phase fault is applied at the Bus 1 and cleared after 0.30 sec. Figure 30 shows the *P-t* curves for this case. From the *P-t* curve of Gen2, the acceleration area A_1 is 0.2531 p.u., and the maximum available declaration area is 0.0774 p.u. This case is decided as an out-of-step condition at 0.50 sec when the total area is 0.1789 p.u. The summary of stable and out-of-step condition simulations for a three-machine infinite-bus system are listed in Table 6.

In summary, the proposed algorithm was not only effective for a SMIB system, but was equally effective for two-machine infinite-bus and three-machine infinite-bus systems also. The proposed algorithm gathered the required data from substations to detect the out-of-step condition. The out-of-step conditions were found directly in the *P-t* domain, and it did not require any network reduction to reduce it to a two-area system. Therefore, this algorithm is fast and effective for application to an *n*-bus system. The proposed

Table 6
Summary of three-machine infinite-bus simulation results

	Case			
	1	2	3	4
Pre-fault load (p.u.)	1.569	1.2189	1.569	1.2189
Fault duration time (sec)	0.1	0.25	0.25	0.30
Generator responsible	Gen2	Gen2	Gen2	Gen2
Acceleration area A_1 (p.u.)	0.0895	0.2127	0.2391	0.2531
Deceleration area A_2 (p.u.)	−0.0895	−0.2127	−0.1204	−0.0774
Maximum deceleration area (p.u.)	−0.1427	−0.3759	−0.1204	−0.0774
$A = A_1 + A_2$	0	0	0.1187	0.1789
Decision time (sec)	0.346	0.519	0.536	0.500
Decision	Stable	Stable	Out-of-step	Out-of-step

algorithm is being tested in a 17-bus system, and a closed loop testing of the algorithm is being done using a real time digital simulator (RTDS^{TM}; RTDS Technologies Inc., Winnipeg, Canada).

4. Conclusion

An algorithm based on energy equilibrium criterion in the time domain is proposed, and its effectiveness is tested for stable swings and out-of-step conditions. The proposed algorithm perfectly discriminates stable and out-of-step swings based on only the local data available from the substation. The algorithm is a real-time algorithm and does not need any off-line calculations. Simulation results showed that the proposed algorithm is also suitable for a wide range of swing frequencies. Results comparing the concentric circle scheme with the proposed scheme show that the new method is much faster. The algorithm also circumvents any need for network reduction of the system.

References

1. Elmore, W. A., *Protective Relaying Theory and Applications*, 2nd ed., New York: Marcel Decker, Inc., 2004.
2. Mason, C. R., *The Art and Science of Protective Relaying*, New York: John Wiley & Sons, Inc., 1958
3. Holbach, J., "New out-of-step blocking algorithm for detecting fast power swing frequencies," *Proceedings of the 30th Annual Western Protective Relay Conference*, Spokane, WA, 21–23 October 2003.
4. Liu, Y., and Lui, Y., "Aspects of power system islanding for preventing widespread blackout," *Proceedings of the IEEE International Conference on Networking, Sensing and Control, 2006 (ICNSC '06)*, pp. 1090–1095, April 2006.
5. Mechraoui, A., and Thomas, D. W. P., "A new principle for high resistance earth fault detection during fast power swings for distance protection," *IEEE Trans. Power Delivery*, Vol. 12, No. 4, pp. 1452–1457, October 1997.
6. Taylor, C. W., Haner, J. M., Hill, L. A., Mittelstadt, W. A., and Cresap, R. L., "A new out-of-step relay with rate of change of apparent resistance augmentation," *IEEE Trans. Power Apparatus Syst.*, Vol. 102, No. 3, pp. 631–639, March 1983.
7. IEEE Power System Relaying Committee of the IEEE Power Engineering Society, "Power swing and out-of-step considerations on transmission line," Report PSRC WG D6, July 2005, available at http://www.pes-psrc.org/Reports/Power%20Swing%20and%20OOS%20Considerations%20on%20Transmission%20Lines%20F.pdf.
8. Tziouvaras, D., and Hou, D., "Out-of-step protection fundamentals and advancements," *Proceedings of the 30th Annual Western Protective Relay Conference*, Spokane, WA, 21–23 October 2003.
9. Abdelaziz, A. Y., Irving, M. R., Mansour, M. M., El-Arabaty, A. M., and Nosseir, A. I., "Adaptive protection strategies for detecting power system out-of-step conditions using neural networks," *IEE Proc. Generat. Transm. Distrib.*, Vol. 145, No. 4, pp. 387–394, July 1998.
10. Rebizant, W., and Feser, K., "Out-of-step protection with AI methods," *IEE 7th International Conference on Developments in Power System Protection*, Publication No. 479, pp. 295–298, 2001.
11. Rebizant, W., and Feser, K., "Fuzzy logic application to out-of-step protection of generators," *IEEE Power Eng. Soc. Summer Mtg.*, Vol. 2, pp. 927–932, 15–19 July 2001.
12. Stevenson, W. D., Jr., *Elements of Power System Analysis*, 4th ed., New York: McGraw Hill, 1982.
13. E. W. Kimbark, *Power System Stability*, Vol. 2, John Wiely and Sons, Inc., New York, 1950.

14. Chen, S., and Sachdev, M. S., "Out-of-step protection using the equal area criterion," *Proceedings of the Canadian Conference on Electrical and Computer Engineering*, Saskatoon, Canada, pp. 1488–1491, 1–4 May 2005.
15. Kundur, P., *Power Stability and Control*, The EPRI Power System Engineering Series, New York: McGraw Hill Inc., 2004.

Appendix A. SMIB Parameters

Base Quantity

Base MVA $= 4 * 550$ MVA
Base kV $= 24$ kV

Generator

MVA rating $= 2220$ MVA
Nominal voltage $= 24$ kV
Direct axis transient reactance $(X'_d) = 0.3$
Inertia constant $(H) = 3.5$ MW-s/MVA
Frequency $= 60$ Hz

Impedances

Transformer $= j0.15$ p.u., TL-I $= j0.5$ p.u., TL-II $= j0.93$ p.u.
Infinite bus: Voltage $= 0.9$ p.u.

Appendix B. Guidelines for Relay Settings

$Z_{base} = \frac{24^2}{2220} = 0.259\Omega$.
RRI = right resistance—inner and is set so that the impedance locus during the most severe stable swing does not cross the inner rectangle. The most severe case is assumed to occur when the generator is fully loaded.
RRO = right resistance—outer and is set so that it is far away from full-load impedance and is less than the impedance at fault removal of the most severe fault.
LRI = same as RRI but in the negative direction.
LRO = same as RRO but in the negative direction.
TXI = set to cover 40% of transmission line.
TXO = set to cover 60% of transmission line.
BX = set to detect swing center passing anywhere in generator and transformer.

Appendix C. Two-machine Infinite-bus Parameters

Base MVA $= 1000$ MVA
Generator-1 rating $= 1000$ MVA
Generator-2 rating $= 1000$ MVA
Bus voltage $= 500$ kV
$Z = 0.6142 + j11.529\ \Omega$

Appendix D. Three-machine Infinite-bus Parameters

Base MVA = 635 MVA
Generator-1 rating = 555 MVA
Generator-2 rating = 635 MVA
Generator-2 rating = 600 MVA
Bus voltage = 24 kV
$Z_1 = 0.048 + j0.48\ \Omega$, $Z_2 = 0.00576 + j0.573\ \Omega$, $Z_3 = 0.0288 + j0.288\ \Omega$
$Z_4 = 0.0576 + j0.576\ \Omega$, $Z_5 = 0.0142 + j0.142\ \Omega$, $Z_6 = 0.0192 + j0.192\ \Omega$
$Z_7 = j0.0957\ \Omega$